

Clay–Organic Hybrid Films Exhibiting Reversible Fluorescent Color Switching Induced by Swelling and Drying of a Clay Mineral

Makoto Tominaga,^{†,‡} Yudai Oniki,[§] Shuhei Mochida,[‡] Kazuo Kasatani,^{§,‡} Seiji Tani,^{§,‡} Yasutaka Suzuki,^{§,‡} Jun Kawamata^{§,‡,}*

[†]Graduate School of Medicine, Yamaguchi University, Yoshida, Yamaguchi 753-8512, Japan

[§]Graduate School of Sciences and Technology for Innovation, Yamaguchi University, Yoshida, Yamaguchi 753-8512, Japan

[‡]Graduate School of Science and Engineering, Yamaguchi University, Yoshida, Yamaguchi 753-8512, Japan

[‡]Research Fellow of Japan Society for the Promotion of Science (DC1)

ABSTRACT: The interlayer space of clays is an interesting microenvironment to control the properties of included organic materials. In this study, chromic hybrid films consisting of synthetic saponite (SSA) and fluorescent organic molecules with planar π -conjugated systems were fabricated. The hybrid films exhibited reversible fluorescence color switching induced by swelling and drying, which caused the gallery height of SSA to change. Ultraviolet–visible absorption, steady-state and time-resolved fluorescence measurements of the hybrid films strongly suggested that the organic molecules formed an excimer in the swollen interlayer space of SSA, while they were a monomer in the dried interlayer space. The different emission wavelengths of the excimer and monomer resulted in the fluorescence color switching of the hybrid films. The reversibility of the color switching was maintained for at least 50 cycles with no change of fluorescence maxima. These chromic hybrid films represent a novel approach to obtain color switching.

INTRODUCTION

Because of the restricted two-dimensional interlayer space of a clay mineral, organic molecules confined in clay–organic hybrid systems often exhibit unique electronic properties that are not observed in their solution or crystalline states. For example, the two-photon absorption cross section of organic molecules with nonplanar conformation is markedly enhanced in synthetic saponite (SSA) compared with that in solution.^{1–3} It was rationalized that the planarity of the π -conjugated system of the confined organic molecule is increased, which extends the π -conjugation length. Another characteristics of organic molecules confined in clay minerals is the enhancement of fluorescence quantum yield.^{4–7} This effect is attributed to the suppression of vibrational motion of the confined molecules.

A clay mineral can accommodate a high density of organic molecules in its interlayer space without aggregation. For example, tetrakis(1-methyl-pyridinium-4-yl)porphyrin (*p*-TMPyP) is known to align without aggregation in the interlayer space of SSA.⁸ In this hybrid, the calculated density of *p*-TMPyP in the total volume of the hybrid was 0.2 mol dm⁻³. Such a high density of intercalated organic molecules with no molecular aggregation and suppressed π – π stacking in these molecular assemblies often results in remarkable energy transfer efficiency between the intercalated molecules.⁹

Another notable characteristic of **smectites, which is a group of clay minerals**, is swelling.^{10–14} Not only pure **smectites** but also clay–organic hybrids can incorporate water or polar organic solvents into their interlayer space. As a result of swelling, the gallery height is expanded compared with that in the dried state. In the swollen state, the surrounding environment of intercalated molecules is different from that in the dried state. Using this property, Takagi et al.¹⁵ demonstrated the switching of the spectroscopic properties **smectite**–organic hybrids. They

reported that the color of a clay–organic hybrid film consisting of [5,10,15,20-tetrakis(*N*-methylpyridinium-4-yl)porphyrinato]tin(IV) and SSA changed remarkably upon swelling. Furthermore, the color of the swollen state depended on the type of solvent used for swelling. This color change was attributed to not conventional solvatochromism caused by the change of dielectric constant but the orientational change of organic molecules resulting from the expansion of the interlayer space.

In this study, we propose a novel color switching mechanism of organic molecules in the interlayer space of **smectites**. In swollen **smectite**–organic hybrids, the gallery height is often expanded to more than 0.8 nm. This interlayer space is large enough for organic molecules to form π – π stacking interactions because it is about twice the thickness of a planar π -conjugated system. Consequently, the organic molecules that exist in monomer form with high density in the dried **smectite**–organic hybrid should be able to form π – π stacking interactions in the swollen state. The swollen interlayer space may be shrunk to the original interlayer space by drying. Therefore, simply by drying the swollen **smectite**–organic hybrid, the intercalated organic molecules should rearrange into their original monomer form even when the molecules form π – π stacking arrangements in the swollen state. If such switching between π – π -stacked and monomeric organic molecules can be realized, the spectroscopic properties of the intercalated organic molecule should be modified as a result.

We aimed to form and break π – π stacking interactions of the confined organic molecules in the interlayer space of a **smectite** by adding and removing a polar solvent, respectively. Among the specific characteristics of π – π -stacked molecules, we focused on the formation and deconstruction of excimers. Typically, an excimer is formed by the π – π interactions between fluorescent organic molecules with a planar π -conjugated system at high concentration. For

example, it is known that pyrene forms an excimer¹⁶ in a solution of methylcyclohexane at concentrations higher than 1 mmol dm⁻³. Because the energy gap of the excimer is smaller than that of monomer,^{17,18} fluorescence is drastically red-shifted.

In this study, we fabricate **smectite**–organic hybrid films consisting of SSA and five fluorescent organic molecules with a planar π -conjugated system. The **smectite**–organic hybrid films with an appropriate density of organic molecules exhibit fluorescence attributed to the monomer in the dried state. By adding a polar solvent to the films, considerable red shifts of fluorescence that could be attributed to the formation of excimers are observed. Upon removing the solvent, fluorescence returns to the original color. This reversible fluorescent color change can occur at least 50 times with no change of the fluorescence maxima. The investigated systems might allow the possibility to develop films that display switching under mild external stimuli.

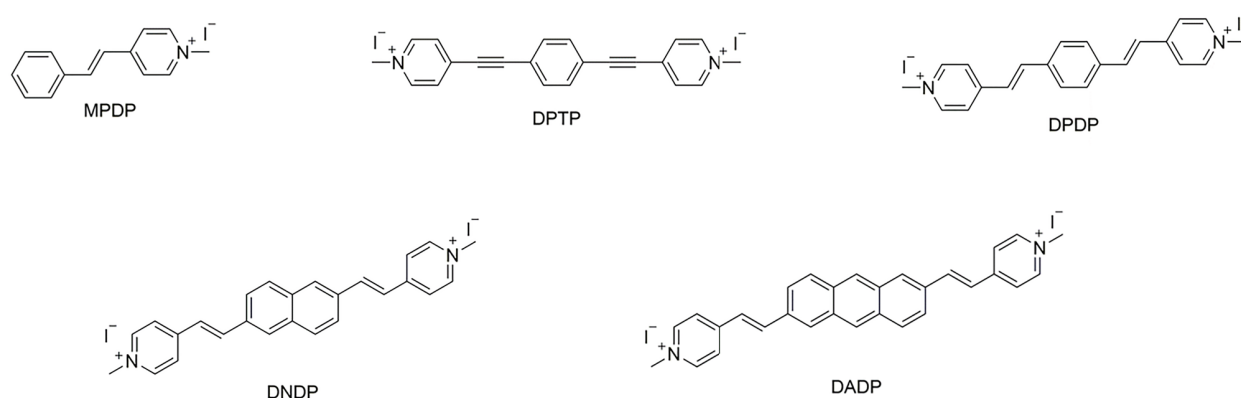


Figure 1. Chemical structures of the fluorescent organic molecules with planar π -conjugated systems used in **smectite**–organic hybrid films.

EXPERIMENTAL SECTION

Organic Molecules. The fluorescent organic cationic molecules with planar π -conjugated systems used in this study were 1-methyl-4-[(1E)-2-phenylethenyl]pyridinium iodide (MPDP),

4,4'-[4,1-phenylenedi-2,1-ethynediyl]bis[1-methylpyridinium] diiodide (DPTP), 4,4'-[4,1-phenylenedi-(1*E*)-2,1-ethenediyl]bis[1-methylpyridinium] diiodide (DPDP), 4,4'-[2,6-naphthylenedi-(1*E*)-2,1-ethenediyl]bis[1-methylpyridinium] diiodide (DNNDP), and 4,4'-[2,6-anthrylenedi-(1*E*)-2,1-ethenediyl]bis[1-methylpyridinium] diiodide (DADP). The structures of these molecules are shown in Figure 1. DPTP,¹ DNNDP,¹⁹ and DADP¹⁹ were synthesized according to our previous reports. MPDP and DPDP were synthesized as follows and characterized by ¹H nuclear magnetic resonance (NMR) spectroscopy measured with a Bruker BioSpin Avance 400 spectrometer.

Synthesis of MPDP. Benzaldehyde (0.55 g, 5.2 mmol) and 1,4-dimethylpyridinium iodide (1.18 g, 5.0 mmol) were dissolved in ethanol (20 mL). Piperidine (10 drops) was dropped into the reaction mixture and then the mixture was stirred for 24 h at 80 °C. The precipitate was collected by filtration and recrystallized from ethanol to obtain MPDP as a yellow solid (50%). ¹H NMR (400 MHz, DMSO-*d*₆, ppm), δ = 8.88 (d, *J* = 6.8 Hz, 2H, pyridyl), 8.24 (d, *J* = 6.8 Hz, 2H, pyridyl), 8.02 (d, *J* = 16.4 Hz, 1H, ethenyl), 7.77 (d, *J* = 6.8 Hz, 2H, phenyl), 7.54 (d, *J* = 16.4 Hz, 1H, ethenyl), 7.51–7.48 (m, 3H, phenyl), 4.27 (s, 3H, -CH₃).

Synthesis of DPDP. First, 1,4-benzenedicarboxaldehyde (0.34 g, 2.5 mmol) and 1,4-dimethylpyridinium iodide (1.18 g, 5.0 mmol) were dissolved in ethanol (20 mL). Piperidine was then dropped into the reaction mixture. The mixture was stirred for 7 h at 80 °C. The resulting precipitate was collected by filtration and recrystallized from water to obtain DPDP as a yellow solid (54%). ¹H NMR (400 MHz, DMSO-*d*₆, ppm), δ = 8.89 (d, *J* = 6.8 Hz, 4H, pyridyl), 8.24 (d, *J* = 6.8 Hz, 4H, pyridyl), 8.04 (d, *J* = 16.4 Hz, 2H, ethenyl), 7.87 (s, 4H, phenyl), 7.63 (d, *J* = 16.4 Hz, 2H, ethenyl), 4.27 (s, 6H, -CH₃).

Clay Minerals. In this study, SSA (Sumecton SA, Kunimine Industries) provided by the Clay Science Society of Japan was selected as a host clay mineral. This is because this SSA does not contain Fe^{3+} , which is expected to quench the fluorescence from the confined molecules. The stoichiometric formula of this SSA is $[(\text{Si}_{7.20}\text{Al}_{0.80})(\text{Mg}_{5.97}\text{Al}_{0.03})\text{O}_{20}(\text{OH})_4]^{0.77-} \cdot (\text{Na}_{0.49}\text{Mg}_{0.14})^{0.77+}$, and it has a cation exchange capacity (CEC) of 0.997 mEq g^{-1} .²⁰

Fabrication of SSA–Organic Hybrid Films. SSA–organic hybrids were prepared by mixing an aqueous dispersion of SSA with an aqueous solution of an organic molecule. Hybrid films were prepared by filtering the aqueous dispersions of SSA–organic hybrids under suction through a mixed cellulose ester membrane filter (Advantec, A010A025A; pore size: 100 nm; diameter: 25 mm) as described in our previous paper.²¹ The resulting hybrid films were washed with ethanol and then air dried. Table S1 lists the values used to prepare optimized SSA–organic hybrids. The thickness of all hybrid films determined from measurement of their interference fringe patterns was ca. $0.4 \mu\text{m}$. The loading level, which is described as %CEC of organic molecules in a SSA–organic hybrid film, was defined as the ratio of organic molecules to the CEC of the clay mineral.

X-ray Diffraction Measurements. X-ray diffraction (XRD) data were collected using a Rigaku Ultima-IV diffractometer with monochromatized $\text{Cu K}\alpha$ radiation ($\lambda=0.154 \text{ nm}$).

Measurement of UV-vis Spectra. Absorption spectra of organic molecules in solution were measured with a UV-vis spectrometer (JASCO, U-670) using optical path lengths of 1 mm for concentrations of 1.0×10^{-3} and $1.0 \times 10^{-4} \text{ mol dm}^{-3}$ and 10 mm for 1.0×10^{-5} , 1.0×10^{-6} and $1.0 \times 10^{-7} \text{ mol dm}^{-3}$. Dimethyl sulfoxide (DMSO) was used as a solvent. The same spectrometer equipped with an attachment for films (JASCO, VTA-752) was used to measure absorption spectra of the SSA–organic hybrid films.

Measurement of Fluorescence Spectra and Quantum Yields. Fluorescence spectra and quantum yields of organic molecules in DMSO and the SSA–organic hybrid films were measured with an absolute photoluminescence quantum yield measurement system (Hamamatsu Photonics, C9920-02G). The fluorescence spectra of the organic molecules in DMSO were measured using a concentration of 1.0×10^{-6} mol dm⁻³.

Time-Resolved Fluorescence Measurements. Time-resolved fluorescence measurements of the SSA–organic hybrid films were conducted using a streak scope (Hamamatsu Photonics, C4334) under photon-counting conditions. The second harmonic (390 nm) of a femtosecond Ti:sapphire laser (Spectra-Physics, Tsunami) equipped with a pulse selector (Spectra-Physics, Model 3980) was used as the excitation source. The pulse duration was 120 fs and the resulting repetition rate was 4 MHz. The maximum average incident power was 0.3 mW.

Swelling and Drying of SSA–Organic Hybrid Films. The nonvolatile polar solvent DMSO was used to swell the SSA–organic hybrid films. Because DMSO is nonvolatile, the swollen states of the films were stable enough to characterize their physical and optical properties. **The spectral change accompanied by swelling/drying was essentially the same even when the other solvents, water, methanol, ethanol and DMF, were employed. This means the organic molecules employed in this study do not have any specific interaction with DMSO.**

The removal of DMSO from the swollen SSA–organic hybrids was conducted as follows. First, the SSA–organic hybrid films were washed with ethanol. Second, the SSA–organic hybrid films were air dried to remove the ethanol.

Density Functional Theory Calculations. All density functional theory²² (DFT) calculations were performed with the Gaussian 09 program package.²³ The geometry of DPDP in the ground state (S_0), belonging to the C_2 point group, in the presence of a solvent was fully optimized using

the hybrid functional B3LYP^{24,25} in conjunction with the 6-31++G(d,p) basis set.²⁶⁻²⁹ The effects of solvent on geometry were taken into account by means of the polarizable continuum model³⁰ (PCM) using the integral equation formalism³¹⁻³³ (IEF-PCM). The absorption properties of the DPDP monomer at the optimized geometry in vacuo and in DMSO were obtained using the time-dependent density functional theory³⁴⁻⁴⁰ (TD-DFT) method at the B3LYP/6-31++G(d,p) level of theory with the IEF-PCM model; excitation energies, transition dipole moments, and oscillator strengths between the ground state and ten lowest-energy singlet excited states were calculated. The geometry of the DPDP dimer in the lowest-energy singlet excited state (S_1), belonging to the C_1 point group, was also fully optimized by the TD-DFT method at the B3LYP/6-31++G(d,p) level of theory with the IEF-PCM model. The B3LYP hybrid functional was selected because it has been reported that the geometry of benzene in S_0 obtained at the B3LYP/6-31+G(d) level of theory agrees well with the experimental geometry,⁴¹ and the TD-DFT method at the B3LYP/6-31+G(d) level reasonably reproduces the low-lying singlet excited states of the benzene monomer.³⁶ Based on these previous reports, in this study, the larger 6-31++G(d, p) basis set was used because DPDP is more polar than benzene. Surfaces of molecular orbitals associated with the electronic transitions were generated and visualized with GaussView 5.0.9 (Gaussian, Inc.).

RESULTS AND DISCUSSION

Figure 2 shows the absorption spectra of a DMSO solution (10^{-4} mol dm^{-3}) of DPDP and SSA-DPDP hybrid film at 1%CEC. The solubility of DPDP in DMSO was ca. 2.0×10^{-3} mol dm^{-3} . DPDP in DMSO exhibited an absorption peak at 398 nm with a shoulder at about 420 nm. No meaningful change was observed for the absorption spectra of DPDP in DMSO solution

within the concentration range of 10^{-3} – 10^{-7} mol dm⁻³ (Figure S1). This indicates that DPDP is a monomer in DMSO even in the saturated solution. In contrast, the SSA–DPDP hybrid film at 1%CEC exhibited two absorption peaks at 417 and 441 nm. The peak observed at about 540 nm was not caused by the light absorption of DPDP, but by the interference fringe pattern of light. **Actually, no fluorescence was observed from a SSA-DPDP hybrid film with 1%CEC even when the film was excited at 540 nm. Such pseudo peak** is often observed in thin films with excellent surface planarity. The absorption band of DPDP in the SSA film was red-shifted compared with that in DMSO. The absorption spectra of organic molecules are often red-shifted when they are intercalated into the interlayer space of clay minerals **because of the enhancement of the planarity of the intercalated molecule and/or the hydrophobic environment of the interlayer space of a clay mineral.**^{42,43} For example, Nile red, which is an organic molecule with a planar π -conjugated system like DPDP, is confined as a monomer in the interlayer space of SSA and its absorption peak in hybrid films is red-shifted by ca. 49 nm compared with that of the monomer in solution.⁴⁴ **Although the spectral shift accompanies change of the shape of absorption spectra, such spectral change is often observed for other molecules reported in references 7, 8, 45. The reason is attributed mainly to the change of microenvironments of confined molecule as can be seen in references 7, 8, 45.** Thus, DPDP is thought to be isolated as a monomer in the hybrid film like it is in the DMSO solution.

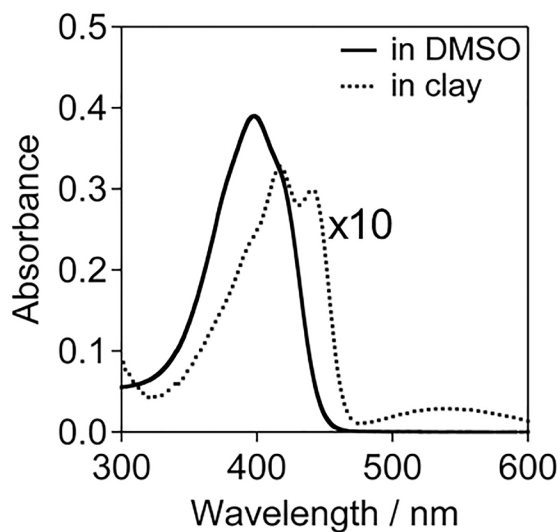


Figure 2. Absorption spectra of DPDP in DMSO solution (10^{-4} mol dm $^{-3}$) and a SSA–DPDP hybrid film at 1%CEC.

Figure 3 shows the absorption spectra of SSA–DPDP hybrid films with a thickness of 0.4 μ m and various %CEC. The absorbance of the film with 0.05%CEC was too low to be observed at this thickness. Therefore, the absorption maximum of the film with 0.05%CEC shown in Table 1 was estimated from the spectrum of a film with 0.05%CEC and a thickness of 1.3 μ m (Figure S2). The absorption spectra of SSA–DPDP hybrid films with lower than 10%CEC were almost the same as each other. For SSA–DPDP hybrid films with higher than 20%CEC, the absorption spectra displayed a gradual blue shift with increasing loading level of DPDP. The absorbance of the peaks at around 440 nm relative to those at around 410 nm decreased as the loading level increased. **The main reason can be attributed to the partial formation of H-aggregates upon increasing the loading level, but microenvironmental change of confined organic molecules may be considered.**^{46–49}

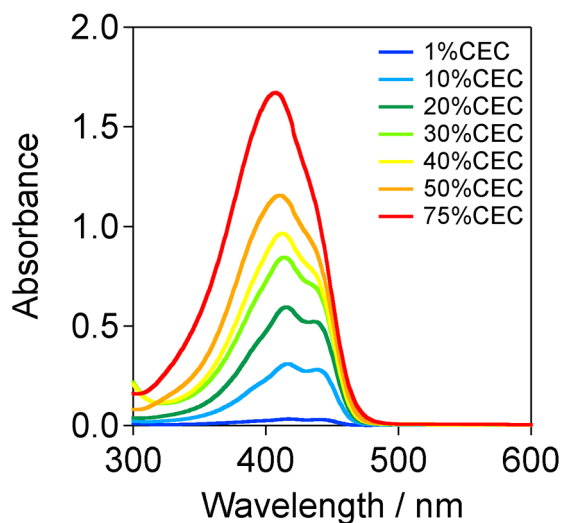


Figure 3. Absorption spectra of SSA–DPDP hybrid films with various loading levels (%CEC).

The thickness of the hybrid films was ca. 0.4 μm .

Table 1. Absorption Maxima of SSA–DPDP Hybrid Films with Various %CEC

%CEC	$\lambda_{\text{max}}^{\text{abs}} / \text{nm}$
0.05	418, 438
1	417, 441
10	416, 439
20	415, 437
30	414, 435
40	412, 433
50	410, 429
75	407, 424

Figure 4(a) shows the fluorescence spectra of a DMSO solution ($10^{-5} \text{ mol dm}^{-3}$) and saturated DMSO solution ($1.4 \times 10^{-3} \text{ mol dm}^{-3}$) of DPDP, which displayed maximum fluorescence wavelengths of 482 and 493 nm, respectively. Although the maximum fluorescence wavelength red-shifted as the concentration of DPDP in DMSO solution increased, the cutoff wavelength remained unchanged. Therefore, the observed red shift could be attributed to the reabsorption effect.^{50,51} Thus, no meaningful changes were observed in the absorption and

fluorescence spectra of DPDP in DMSO solutions even when its concentration was varied. These observations indicate that DPDP existed as a monomer and did not form an excimer in DMSO at any concentration.

Figure 4(b) depicts the fluorescence spectra of as-prepared SSA-DPDP hybrid films with various %CEC. Table 2 lists the maximum fluorescence wavelengths and fluorescence quantum yields of these films together with those in DMSO. The fluorescence quantum yield of DPDP was considerably enhanced by confinement in a clay mineral. Similar drastic enhancement also reported for other organic molecules.^{4,7} The reason is attributed to the suppression of vibrational motion of the confined molecules. The SSA–DPDP hybrid film with 0.05%CEC exhibited fluorescence peaks at 464 and 489 nm. Relative intensity of the peak observed at a shorter wavelength was gradually decreased as time elapsed from fabrication. Therefore, the shorter wavelength component of fluorescence is attributed to that from some part of organic molecules adsorbed on a clay in meta-stable manner. The wavelength of the peak observed at 489 nm was 7 nm longer than that in solution. Considering the red shift of absorption spectra by the confinement, the red shift of fluorescence spectra can also be attributed to the change of microenvironment of the DPDP molecule. Thus, DPDP should be confined in the interlayer space of SSA in a monomer form at this loading level. Fluorescence from a SSA–DPDP hybrid film with 1%CEC was also assigned to the DPDP monomer because the absorption maxima and fluorescence quantum yield were similar to those observed for a film with 0.05%CEC. Although the emission and absorption maxima observed for a film with 10%CEC were almost the same as those of the film with 1%CEC, the fluorescence quantum yield of the film with 10%CEC was almost half those of films with lower than 1%CEC. Organic molecules confined in the interlayer space of a clay mineral tend to form a partial H-aggregation even at a few %CEC.^{8,45} Thus, the

decrease of fluorescence quantum yield strongly suggests the partial formation of H-aggregates of DPDP in films with higher than 10%CEC because typical H-aggregates are not fluorescent.^{52,53} Fluorescence quantum yield gradually decreased as the loading level of DPDP was increased from 10%CEC to 40%CEC. The absorption behavior indicates that the percentage of H-aggregate in the interlayer of SSA becomes higher with increasing loading level of DPDP, and fluorescence was observed only from the monomer form of DPDP. These considerations are consistent with the similar fluorescence wavelengths for the film with lower than 40%CEC, and thus only the molecules confined in a monomer form emit fluorescence. However, the shape of fluorescence spectra changed slightly as the loading level varied. The fluorescence component centered at 464 nm became weaker as the loading level was increased from 0.05%CEC to 40%CEC. This is thought to be caused by the reabsorption effect. For the film with 50%CEC, a new fluorescent component was observed at around 588 nm in addition to the monomer components. For the SSA–DPDP hybrid film with 75%CEC, only the fluorescent component at 588 nm was observed. The absorption spectra of the hybrid films with higher than 50%CEC were similar to those of the hybrid films with lower than 40%CEC. Nevertheless, on increasing the loading level, a new fluorescent component at much longer wavelength than those of the monomer components appeared. This observation strongly suggests that excimers formed in the films with a high DPDP loading. We conducted time-resolved fluorescence measurements of the films (Figure S3). The fluorescent lifetime measured for the peak at 588 nm was 18 times longer than that of the monomer fluorescence. This observation also supports the formation of excimers.

Here, let us estimate the surface coverage of DPDP on SSA. As shown in Figure 5, the surface coverage represents the percentage of the surface of a single clay layer covered by organic molecules. The surface coverage is calculated as²

$$\text{coverage (\%)} = \frac{\% \text{CEC} \times \text{cross-sectional area of an organic molecule per cationic moiety}}{\text{surface area of SSA per anionic site}}$$

When the coverage is 100%, both sides of the clay surface are fully covered with the confined molecules. In a hybrid film, each interlayer space is formed between two clay layers. Thus, the space-filling percentage (Figure 5) of the interlayer space is 100% when clay layers with a surface coverage of 50% are stacked. Because the estimated cross-sectional area of DPDP viewed normal to the π -electron system is about 1.4 nm² (Figure S4), the cross-sectional area per cationic moiety is 0.7 nm². The calculated surface area per anionic site of SSA is 1.3 nm². The surface coverage of the 50%CEC hybrid film is 29%. Therefore, 58% of the interlayer space of SSA is filled by DPDP in this film. As mentioned above, organic molecules tend to segregate in the interlayer space of clay minerals.⁵⁴ It has been reported that partial exchange of cations in clay minerals always occurs in a segregated manner, producing random interstratifications.⁵⁵ This means there should be large variation of the space-filling percentage in each interlayer space in actual hybrid films. Therefore, it is not surprising that excimers form if a particular interlayer space is filled with DPDP with an average space-filling percentage higher than 50%. The average density of DPDP in the interlayer space of the hybrid film with 50%CEC was estimated to be 1.44 mol dm⁻³. This value is about 1000 times higher than the concentration of the saturated solution of DPDP in DMSO. Therefore, it is reasonable that DPDP excimers formed at such high density.

Figure 4(c) presents the fluorescence spectra of SSA–DPDP hybrid films in a swollen state. The maximum fluorescence wavelengths and fluorescence quantum yields are also summarized in Table 2. For the SSA–DPDP hybrid film with 0.05%CEC, fluorescence was observed mainly from the monomer at 464 and 487 nm, although a weak peak was observed from the excimer at 580 nm. For the SSA–DPDP hybrid film with 1%CEC, the dominant fluorescence peak was

from the excimer at 583 nm. For the SSA–DPDP hybrid films with higher than 10%CEC, only excimer emission was observed. These results indicate that excimer formation in the swollen interlayer space of SSA occurred even at a lower %CEC than in the as-prepared films.

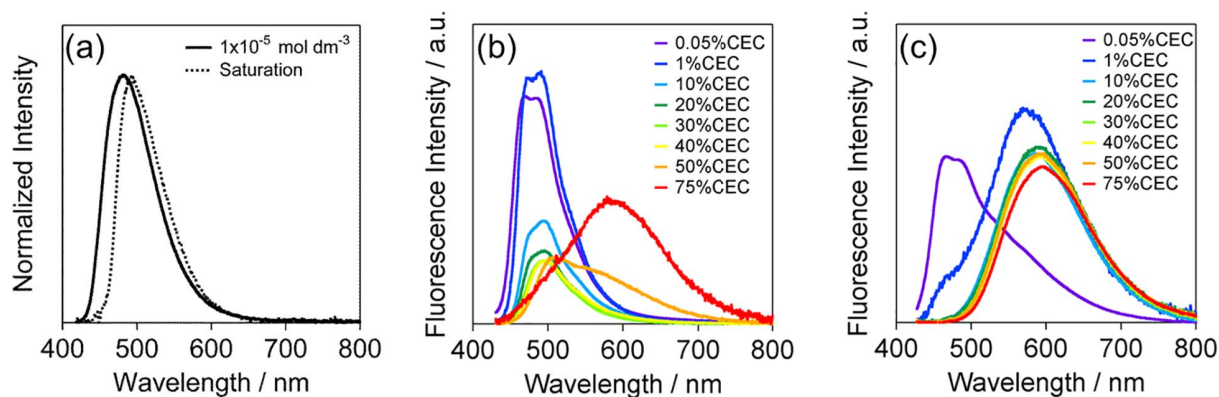


Figure 4. Fluorescence spectra of (a) DMSO solutions of DPDP, (b) as-prepared SSA–DPDP hybrid films, and (c) SSA–DPDP hybrid films in the swollen state.

Table 2. Fluorescence Maxima and Fluorescence Quantum Yields of SSA-DPDP Hybrid Films and DPDP in DMSO

	concentration / mol dm ⁻³	$\lambda_{\text{max}}^{\text{em}}$ / nm		ϕ	
in DMSO	10 ⁻⁵	482		0.06	
	%CEC	as-prepared	swollen	as-prepared	swollen
	0.05	464, 489	464, 487	0.67	0.49
	1	472, 490	471, 583	0.75	0.63
	10	474, 495	587	0.31	0.51
	20	480, 495	590	0.22	0.53
in SSA	30	495	590	0.19	0.51
	40	496	594	0.19	0.50
	50	505, 560	596	0.20	0.51
	75	588	596	0.37	0.47

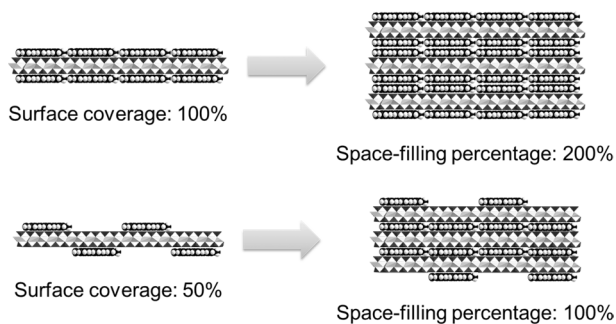


Figure 5. Schematic representation of the relationship between surface coverage and space-filling percentage.

The fluorescent color change of the hybrid films with different CEC is depicted in Figure 6. For the film with an extremely low %CEC of 0.05%, only monomer emission was observed even in the swollen state. In contrast, for films with higher than 50%CEC, only excimer emission was detected even in the as-prepared state. However, for the films with 10%CEC–40%CEC, monomer emission occurred in the as-prepared state and excimer emission in the swollen state. By optimizing the density of DPDP in the interlayer space of SSA, hybrid films that exhibit fluorescence switching between monomer emission in the as-prepared state and excimer emission in the swollen state can be fabricated.

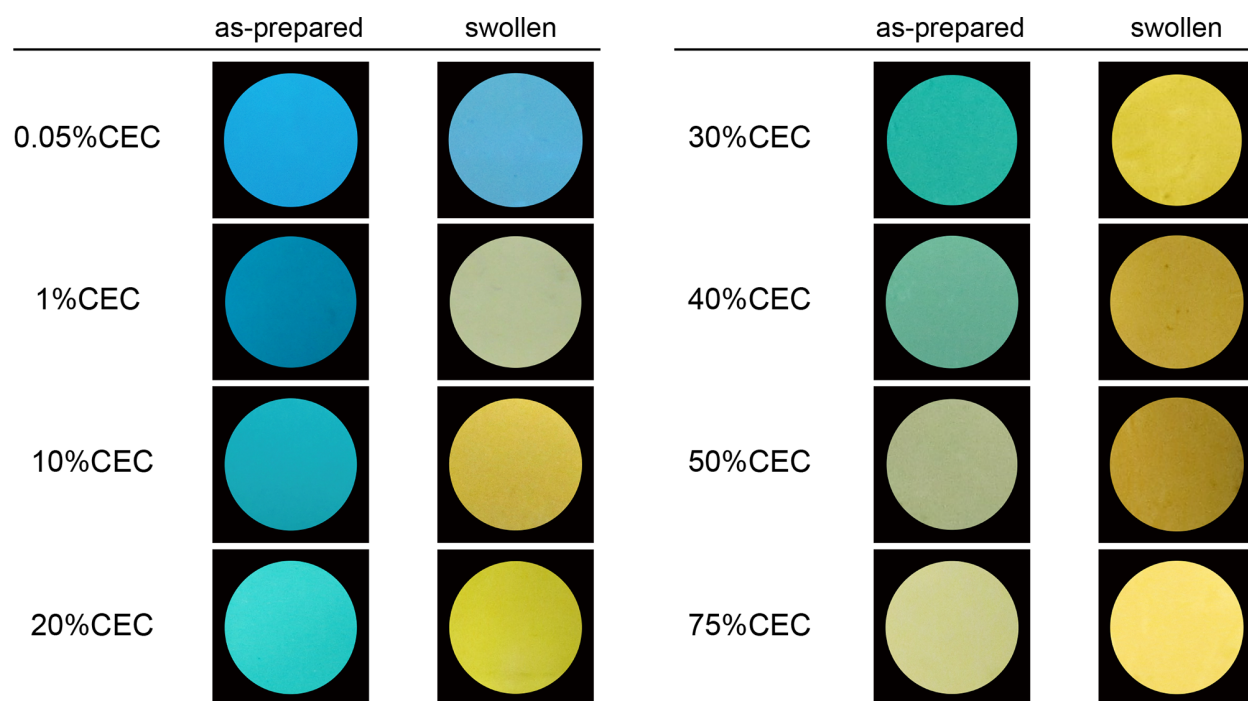


Figure 6. Fluorescence colors of SSA–DPDP hybrid films with various %CEC loading. Left and right columns correspond to the as-prepared and swollen states, respectively.

To investigate the environmental change of the interlayer space accompanied by swelling, the SSA–DPDP hybrid film with 10%CEC that exhibited a remarkable fluorescent color change upon swelling was examined by XRD. The gallery height of this SSA–DPDP hybrid film in the as-prepared state was 0.48 nm. This value is almost the same as the thickness of DPDP viewed parallel to the π -conjugated system. In the swollen state, the gallery height of the SSA–DPDP hybrid film with 10%CEC was 0.93 nm, which is almost twice the thickness of DPDP. This means that the interlayer space of swollen SSA is large enough for DPDP to form π – π stacking interactions.

DFT and TD-DFT calculations were carried out to support the observed spectroscopic behavior and predict the geometry of DPDP in the swollen interlayer space. The spectroscopic properties of the optimized DPDP monomer were calculated using TD-DFT at the B3LYP/6-

31++G(d,p) level of theory. From the harmonic vibrational analysis of the optimized DPDP monomer in S_0 , it was confirmed that the optimized geometry belonging to the C_2 point group was the stationary point corresponding to energy minima on the potential energy surface of S_0 . Absorption ($S_0 \rightarrow S_1$) wavelengths λ , singlet excitation energies E , and oscillator strengths f of the DPDP monomer in vacuo and in DMSO are summarized in Table 3. E in vacuo is similar to that in DMSO. This suggests that the effect of solvent on E is negligible. The calculated E for DPDP monomers in DMSO is 2.67 eV at the same level of theory, which agrees well with the experimental value (2.95 eV) for DPDP monomers in DMSO. The geometry of a DPDP dimer in S_1 in DMSO was also optimized using TD-DFT at the B3LYP/6-31++G(d,p) level of theory. The obtained geometry of the DPDP excimer is different from the equilibrium geometry of the DPDP dimer in S_0 ; i.e., it is not a stationary point corresponding to the energy minimum on the potential energy surface of S_0 . Table 3 also lists λ and E of the DPDP excimer. The calculated E of the DPDP excimer in DMSO is 1.92 eV. This calculated value shows good agreement with the experimental one (2.13 eV) for a SSA–DPDP hybrid film in the swollen state. Therefore, our experimental results are reproduced well by the DFT and TD-DFT calculations. The geometry of the DPDP excimer (S_1) in DMSO and the surfaces of its highest occupied molecular orbital (HOMO) and lowest unoccupied molecular orbital (LUMO) are shown in Figure 7 and Figure 8, respectively. The interplanar distance between the two benzene rings, twist angle between the long axes of DPDP molecules, and the parallel translation of the benzene ring of one molecule relative to the benzene ring of the other nearly along the long axis of the monomer are 3.53 Å, 0.15°, and 2.50 Å, respectively. Considering the van der Waals radii of the optimized DPDP excimer, its thickness is 7.13 Å. This value is smaller than the gallery height of the SSA–DPDP hybrid film in the swollen state but larger than that in the dried state. Therefore, the geometry of

the DPDP excimer calculated with the TD-DFT method may reflect the structure of the DPDP excimer in the swollen interlayer space of SSA.

Table 3. Comparison of Calculated and Experimental Absorption ($S_0 \rightarrow S_1$) Wavelengths (λ), Singlet Excitation Energies (E), and Oscillator Strength (f) of DPDP Monomer and Excimer

	solvent	calculated ^a			experimental		
		λ / nm	E / eV	f	λ / nm	E / eV	f
DPDP monomer	in vacuo	457	2.71	1.92			
	DMSO	465	2.67	2.04	420	29.5	0.77
DPDP excimer	DMSO	645	1.92		583	2.13	

^aCalculated using the hybrid B3LYP functional with the 6-31++G(d,p) basis set.

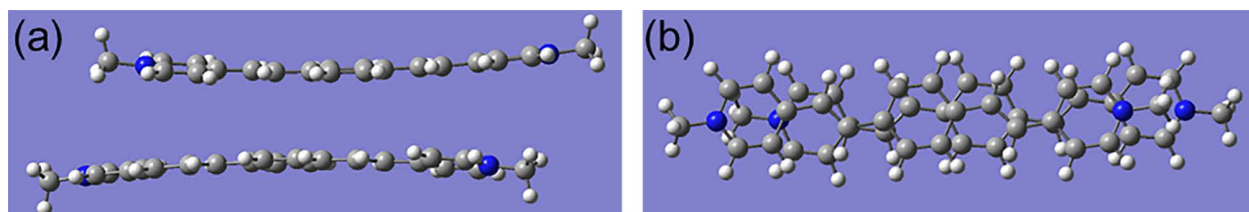


Figure 7. The geometry of a DPDP excimer (S_1) in DMSO calculated at the B3LYP/6-31++G(d,p) level. (a) Side view, and (b) top view.

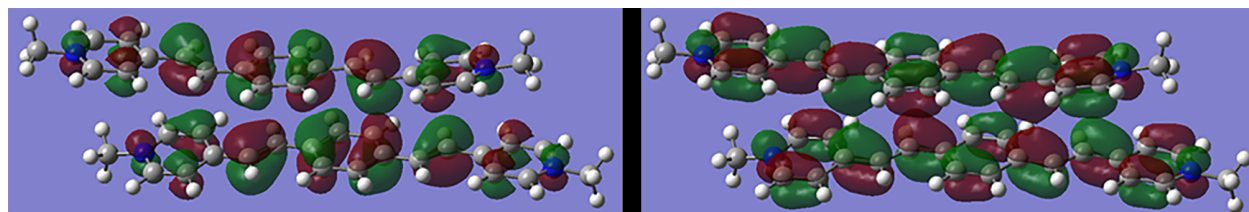


Figure 8. Surfaces of the highest occupied molecular orbital (HOMO, left) and lowest unoccupied molecular orbital (LUMO, right) of a DPDP excimer (S_1) in DMSO calculated at the B3LYP/6-31++G(d,p) level.

We fabricated hybrid films consisting of SSA and other fluorescent molecules that tend to form π - π stacking arrangements. Similar switching of fluorescent color accompanied by swelling to that found for the SSA-DPDP films was observed for these films containing other fluorescent molecules. Figure 9 compares the fluorescence colors of as-prepared and swollen SSA-MPDP, SSA-DPTP, SSA-DPDP, SSA-DNDP, and SSA-DADP hybrid films with 10%CEC. The emission wavelengths and the quantum yields of these hybrid films are summarized in Table 4. All the planar fluorescent molecules exhibited fluorescence color switching in the interlayer space of SSA upon swelling. The wavelength shift of fluorescence peaks for these films ranged from 35 to 92 nm. In contrast, absorption peaks did not shift markedly upon swelling (Table 4). In addition, fluorescence lifetimes of these films in the swollen state were considerably longer than those in the as-prepared state (Figure S5). Thus, the fluorescence color changes observed for these films can also be attributed to the formation of excimers following swelling. As in the case of DPDP, none of these molecules exhibited excimer emission in their saturated solutions. Thus, by utilizing the swelling-controlled interlayer environment of clay minerals, fluorescence characteristics of planar fluorescent organic molecules can easily be switched.

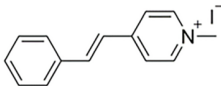
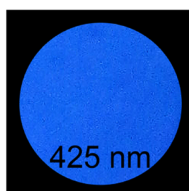
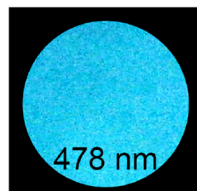
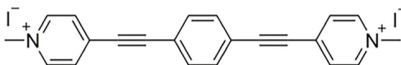
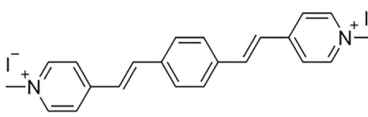
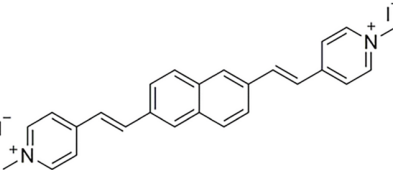
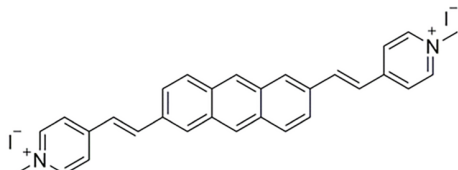
	chemical structure	as-prepared	swollen
(a) SSA-MPDP			
(b) SSA-DPTP			
(c) SSA-DPDP			
(d) SSA-DNDP			
(e) SSA-DADP			

Figure 9. Fluorescence color changes of (a) SSA–MPDP, (b) SSA–DPTP, (c) SSA–DPDP, (d) SSA–DNDP, and (e) SSA–DADP hybrid films with 10%CEC induced by swelling. Left and right columns correspond to the as-prepared and swollen states, respectively. The values in photographs are wavelengths of fluorescence maxima.

Table 4. Absorption, Fluorescence Maxima and Fluorescence Quantum Yields of SSA–MPDP, SSA–DPTP, SSA–DPDP, SSA–DNDP and SSA–DADP Hybrid Films with 10% CEC

sample	$\lambda_{\max}^{\text{abs}}$ / nm	$\lambda_{\max}^{\text{em}}$ / nm	$\Delta \lambda_{\max}^{\text{em}}$ / nm	ϕ
--------	------------------------------------	-----------------------------------	--	--------

	as-prepared	swollen	as-prepared	swollen		as-prepared	swollen
SSA–MPDP	345	362	425	478	53	0.05	0.08
SSA–DPTP	353	393	449	511	62	0.46	0.23
SSA–DPDP	416, 439	399	495	587	92	0.31	0.51
SSA–DNDP	381, 424	433, 456	531	598	67	0.32	0.47
SSA–DADP	356, 393, 413, 472	364, 404, 425, 515	603	638	35	0.27	0.21

The interlayer spacing of swollen organic–clay hybrids readily returns to the initial spacing upon drying.⁵⁶ Therefore, we examined fluorescence color change of a film that was dried after swelling. Figure 10 illustrates the fluorescence colors of a SSA–DPDP hybrid film in the as-prepared, swollen, and dried states. The yellow fluorescence of the swollen SSA–DPDP hybrid film recovered to the blue-green emission of the as-prepared SSA–DPDP hybrid film. All hybrid films fabricated in this study exhibited such reversible color changes.



Figure 10. Fluorescence colors of a SSA–DPDP hybrid film in the as-prepared state (left), swollen state (middle), and dried state (right).

We investigated the repeatability of the fluorescence color switching of the hybrid films. Figure 11 exemplifies the variation of the fluorescence maxima of a SSA–DPDP hybrid film in the dried and swollen states. By repeatedly adding and removing DMSO, reversible fluorescence color changes with almost the same wavelength change were observed for at least 50 cycles. This reversible fluorescence color change between monomer and excimer emission was observed for all the SSA–organic hybrid films used in this study. The mechanism of this color change does not involve the structural change of an organic molecule. Only a mild stimulus, namely addition and removal of solvent, is needed to induce such a substantial color change. This approach of

inducing a specific molecular assembly in the interlayer space of a clay mineral provides a novel chromic system that displays high repeatability.

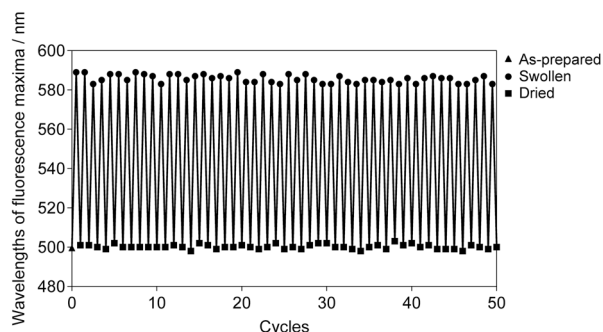


Figure 11. Reversibility of the wavelengths of fluorescence maxima of a SSA–DPDP hybrid film in dried and swollen states.

CONCLUSIONS

In this study, we developed chromic films that exhibited reversible fluorescent color changes between monomer and excimer emission with high repeatability. This phenomenon was achieved by switching the degree of confinement of organic molecules in the interlayer space of a **smectite** between the dried and swollen states. By controlling the environment in the interlayer space, we demonstrated formation and deconstruction of the excimer under a mild external stimulus. This environmental switching of the interlayer space of a clay mineral can be used to switch other physical properties of included materials. The swelling properties of **smectite**–organic hybrids are promising to obtain novel materials that exhibit switching properties.

ASSOCIATED CONTENT

Absorption spectra of DMSO solutions of DPDP (Figure S1) and a SSA–DPDP hybrid film (Figure S2), fluorescence decay curves of SSA–DPDP hybrid films (Figure S3 and S5),

molecular model of DPDP (Figure S4). This material is available free of charge via the Internet at <http://pubs.acs.org>.

AUTHOR INFORMATION

Corresponding Author

* E-mail: j_kawa@yamaguchi-u.ac.jp; Tel/Fax: +81-83-933-5729.

Author Contributions

The manuscript was written through contributions of all authors. All authors have approved the final version of the manuscript.

Notes

The authors declare no competing financial interest.

ACKNOWLEDGMENT

The authors are grateful to Dr. Akihiko Yamagishi for his valuable comments and the Media and Information Technology Center of Yamaguchi University for use of the PC cluster resources for the theoretical calculations. This work was supported by JSPS KAKENHI Grant Numbers 15J07557 and 23510116.

REFERENCES

(1) Kamada, K.; Tanamura, Y.; Ueno, K.; Ohta, K.; Misawa, H. Enhanced Two-Photon Absorption of Chromophores Confined in Two-Dimensional Nanospace. *J. Phys. Chem. C* **2007**, *111*, 11193–11198.

- (2) Suzuki, Y.; Tenma, Y.; Nishioka, Y.; Kamada, K.; Ohta, K.; Kawamata, J. Efficient Two-Photon Absorption Materials Consisting of Cationic Dyes and Clay Minerals. *J. Phys. Chem. C* **2011**, *115*, 20653–20661.
- (3) Suzuki, Y.; Sugihara, H.; Satomi, K.; Tominaga, M.; Mochida, S.; Kawamata, J. Two-Photon Absorption Properties of an Acetylene Derivative Confined in the Interlayer Space of a Smectite. *Appl. Clay Sci.* **2014**, *96*, 116–119.
- (4) Villemure, G.; Detellier, C.; Szabo, A. G. Fluorescence of Clay-Intercalated Methylviologen. *J. Am. Chem. Soc.* **1986**, *108*, 4658–4659.
- (5) Sasai, R.; Itoh, T.; Ohmori, W.; Itoh, H.; Kusunoki, M. Preparation and Characterization of Rhodamine 6G/Alkyltrimethylammonium/Laponite Hybrid Solid Materials with Higher Emission Quantum Yield. *J. Phys. Chem. C* **2009**, *113*, 415–421.
- (6) Bujdák, J.; Iyi, N. Highly Fluorescent Colloids based on Rhodamine 6G, Modified Layered Silicate, and Organic Solvent. *J. Colloid Interface Sci.* **2012**, *388*, 15–20.
- (7) Ishida, Y.; Shimada, T.; Takagi, S. “Surface-Fixation Induced Emission” of Porphyrazine Dye by a Complexation with Inorganic Nanosheets. *J. Phys. Chem. C* **2014**, *118*, 20466–20471.
- (8) Fujimura, T.; Shimada, T.; Hamatani, S.; Onodera, S.; Sasai, R.; Inoue, H.; Takagi, S. High Density Intercalation of Porphyrin into Transparent Clay Membrane without Aggregation. *Langmuir* **2013**, *29*, 5060–5065.
- (9) Ishida, Y.; Shimada, T.; Masui, D.; Inoue, H.; Takagi, S. Efficient Excited Energy Transfer Reaction in Clay/Porphyrin Complex toward an Artificial Light-Harvesting System. *J. Am. Chem. Soc.* **2011**, *133*, 14280–14286.
- (10) Norrish, K. Crystalline Swelling of Montmorillonite: Manner of Swelling of Montmorillonite. *Nature* **1954**, *173*, 256–257.

- (11) Morodome, S.; Kawamura, K. Swelling Behavior of Na- and Ca-Montmorillonite up to 150 °C by In Situ X-ray Diffraction Experiments. *Clays Clay Miner.* **2009**, *57*, 150–160.
- (12) Geng, F.; Ma, R.; Ebina, Y.; Yamauchi, Y.; Miyamoto, N.; Sasaki, T. Gigantic Swelling of Inorganic Layered Materials: A Bridge to Molecularly Thin Two-Dimensional Nanosheets. *J. Am. Chem. Soc.* **2014**, *136*, 5491–5500.
- (13) Lucia, L. A.; Yui, T.; Sasai, R.; Takagi, S.; Takagi, K.; Yoshida, H.; Whitten, D. G.; Inoue, H. Enhanced Aggregation Behavior of Antimony(V) Porphyrins in Polyfluorinated Surfactant/Clay Hybrid Microenvironment. *J. Phys. Chem. C.* **2003**, *107*, 3789–3797.
- (14) Yui, T.; Uppili, S. R.; Shimada, T.; Tryk, D. A.; Yoshida, H.; Inoue, H. Microscopic Structure and Microscopic Environment of a Polyfluorinated Surfactant/Clay Hybrid Compound: Photochemical Studies of Rose Bengal. *Langmuir*, **2002**, *18*, 4232–4239.
- (15) Takagi, S.; Shimada, T.; Masui, D.; Tachibana, H.; Ishida, Y.; Tryk, D. A.; Inoue, H. Unique Solvatochromism of a Membrane Composed of a Cationic Porphyrin–Clay Complex. *Langmuir* **2010**, *26*, 4639–4641.
- (16) Turro, N. J.; Ramamurthy, V.; Scaiano, J. C. *Principles of Molecular Photochemistry: An Introduction*; University Science Books: Sausalito, California, 2009.
- (17) Birks, J. B. *Photophysics of Aromatic Molecules*; Wiley: London, U.K., 1970.
- (18) Beens, H.; Weller, A. *Organic Molecular Physics*; Wiley: London, U.K., 1975.
- (19) Tominaga, M.; Mochida, S.; Sugihara, H.; Satomi, K.; Moritomo, H.; Fuji, A.; Tomoyuki, A.; Suzuki, Y.; Kawamata, J. A Red Fluorescence Two-photon Absorption Probe for Sensitive Imaging of Live Mitochondria. *Chem. Lett.* **2014**, *43*, 1490–1492.
- (20) Takagi, S.; Tryk, D. A.; Inoue, H. Photochemical Energy Transfer of Cationic Porphyrin Complexes on Clay Surface. *J. Phys. Chem. B* **2002**, *106*, 5455–5460.

- (21) Kawamata, J.; Suzuki, Y.; Tenma, Y. Fabrication of Clay Mineral–Dye Composites as Nonlinear Optical Materials. *Philos. Mag.* **2010**, *90*, 2519–2527.
- (22) Kohn, W.; Sham, L. J. Self-Consistent Equations Including Exchange and Correlation Effects. *Phys. Rev. A* **1965**, *140*, 1133–1138.
- (23) Frisch, M. J.; Trucks, G. W.; Schlegel, H. B.; Scuseria, G. E.; Robb, M. A.; Cheeseman, J. R.; Scalmani, G.; Barone, V.; Mennucci, B.; Petersson, G. A.; et al. *Gaussian 09, Rev. D.01*; Gaussian, Inc.: Wallingford CT, U.S.A., 2013.
- (24) Becke, A. D. Density-Functional Thermochemistry. III. The Role of Exact Exchange. *J. Chem. Phys.* **1993**, *98*, 5648–5652.
- (25) Lee, C.; Yang, W.; Parr, R. G. Development of the Colle–Salvetti Correlation-Energy Formula into a Functional of the Electron Density. *Phys. Rev. B* **1988**, *37*, 785–789.
- (26) Ditchfield, R.; Hehre, W. J.; Pople, J. A. Self-Consistent Molecular-Orbital Methods. IX. An Extended Gaussian-Type Basis for Molecular-Orbital Studies of Organic Molecules. *J. Chem. Phys.* **1971**, *54*, 724–728.
- (27) Hehre, W. J.; Ditchfield, R.; Pople, J. A. Self-Consistent Molecular Orbital Methods. XII. Further Extensions of Gaussian-Type Basis Sets for Use in Molecular Orbital Studies of Organic Molecules. *J. Chem. Phys.* **1972**, *56*, 2257–2261.
- (28) Hariharan, P. C.; Pople, J. A. The Influence of Polarization Functions on Molecular Orbital Hydrogenation Energies. *Theor. Chem. Acc.* **1973**, *28*, 213–222.
- (29) Clark, T.; Chandrasekhar, J.; Spitznagel, G. W.; Schleyer, P. V. R. Efficient Diffuse Function-Augmented Basis Sets for Anion Calculations. III. The 3-21+G Basis Set for First-Row Elements, Li–F. *J. Comput. Chem.* **1983**, *4*, 294–301.

- (30) Miertuš, S.; Scrocco, E.; Tomasi, J. Electrostatic Interaction of a Solute with a Continuum. A Direct Utilization of AB Initio Molecular Potentials for the Prevision of Solvent Effects. *Chem. Phys.* **1981**, *55*, 117–129.
- (31) Cancès, E.; Mennucci, B.; Tomasi, J. A New Integral Equation Formalism for the Polarizable Continuum Model: Theoretical Background and Applications to Isotropic and Anisotropic Dielectrics. *J. Chem. Phys.* **1997**, *107*, 3032–3041.
- (32) Mennucci, B.; Cancès, E.; Tomasi, J. Evaluation of Solvent Effects in Isotropic and Anisotropic Dielectrics and in Ionic Solutions with a Unified Integral Equation Method: Theoretical Bases, Computational Implementation, and Numerical Applications. *J. Phys. Chem. B* **1997**, *101*, 10506–10517.
- (33) Cancès, E.; Mennucci, B. New Applications of Integral Equations Methods for Solvation Continuum Models: Ionic Solutions and Liquid Crystals. *J. Math. Chem.* **1998**, *23*, 309–326.
- (34) Bauernschmitt, R.; Ahlrichs, R. Treatment of Electronic Excitations Within the Adiabatic Approximation of Time Dependent Density Functional Theory. *Chem. Phys. Lett.* **1996**, *256*, 454–464.
- (35) Casida, M. E.; Jamorski, C.; Casida, K. C.; Salahub, D. R. Molecular Excitation Energies to High-Lying Bound States from Time-Dependent Density-Functional Response Theory: Characterization and Correction of the Time-Dependent Local Density Approximation Ionization Threshold. *J. Chem. Phys.* **1998**, *108*, 4439–4449.
- (36) Stratmann, R. E.; Scuseria, G. E.; Frisch, M. J. An Efficient Implementation of Time-Dependent Density-Functional Theory for the Calculation of Excitation Energies of Large Molecules. *J. Chem. Phys.* **1998**, *109*, 8218–8224.

- (37) Van Caillie, C.; Amos, R. D. Geometric Derivatives of Excitation Energies using SCF and DFT. *Chem. Phys. Lett.* **1999**, *308*, 249–255.
- (38) Van Caillie, C.; Amos, R. D. Geometric Derivatives of Density Functional Theory Excitation Energies using Gradient-Corrected Functionals. *Chem. Phys. Lett.* **2000**, *317*, 159–164.
- (39) Furche, F.; Ahlrichs, R. Adiabatic Time-Dependent Density Functional Methods for Excited State Properties. *J. Chem. Phys.* **2002**, *117*, 7433–7447.
- (40) Scalmani, G.; Frisch, M. J.; Mennucci, B.; Tomasi, J.; Cammi, R.; Barone, V. Geometries and Properties of Excited States in the Gas Phase and in Solution: Theory and Application of a Time-Dependent Density Functional Theory Polarizable Continuum Model. *J. Chem. Phys.* **2006**, *124*, 094107–094121.
- (41) Amicangelo, J. C. Theoretical Study of the Benzene Excimer Using Time-Dependent Density Functional Theory. *J. Phys. Chem. A* **2005**, *109*, 9174–9182.
- (42) Ishida, Y.; Masui, D.; Shimada, T.; Tachibana, H.; Inoue, H.; Takagi, S. The Mechanism of the Porphyrin Spectral Shift on Inorganic Nanosheets: The Molecular Flattening Induced by the Strong Host-Guest Interaction due to the “Size-Matching Rule”. *J. Phys. Chem. C* **2012**, *116*, 7879–7885.
- (43) Suzuki, Y.; Tenma, Y.; Nishioka, Y.; Kawamata, J. Efficient Nonlinear Optical Properties of Dyes Confined in Interlayer Nanospaces of Clay Minerals. *Chem. Asian. J.* **2012**, *7*, 1170–1179.
- (44) Felbeck, T.; Behnke, T.; Hoffmann, K.; Grabolle, M.; Lezhnina, M. M.; Kynast, U. H.; Resch-Genger, U. Nile-Red-Nanoclay Hybrids: Red Emissive Optical Probes for Use in Aqueous Dispersion. *Langmuir* **2013**, *29*, 11489–11497.

- (45) Suzuki, Y.; Yamamoto, K.; Mikata, K.; Nishioka, Y.; Tani, S.; Kawamata, J. The Size Control of Nano-Cluster Formed on an Inorganic Nanosheet/Cationic Organic Molecule Hybrid Langmuir-Blodgett Film. *J. Nanosci. Nanotechnol.* **2014**, *14*, 2895–2900.
- (46) Iwasaki, M.; Kita, M.; Ito, K.; Kohno, A.; Fukunishi, K. Intercalation Characteristics of 1,1'-Diethyle-2,2'-cyanine and other Cationic Dyes in Synthetic Saponite: Orientation in the Interlayer. *Clays Clay Miner.* **2000**, *48*, 392–399.
- (47) Iyi, N.; Sasai, R.; Fujita, T.; Deguchi, T.; Sota, T.; Arbeloa, F. L.; Kitamura, K. Orientation and Aggregation of Cationic Laser Dyes in a Fluoromica: Polarized Spectrometry Studies. *Appl. Clay Sci.* **2002**, *22*, 125–136.
- (48) Czímerová, A.; Bujdák, J.; Gáplovský, A. The Aggregation of Thionine and Methylene Blue Dye in Smectite Dispersion. *Colloid Surface A* **2004**, *243*, 89–96.
- (49) Hill, E. H.; Zhang, Y.; Whitten, D. G. Aggregation of Cationic *p*-Phenylene Ethynylenes on Laponite Clay in Aqueous Dispersions and Solid Films. *J. Colloid Interface Sci.* **2015**, *449*, 347–356.
- (50) Kaplanová, M.; Cermák, K. Effect of Reabsorption on the Concentration Dependence of Fluorescence Lifetimes of Chlorophyll A. *J. Photochem.* **1981**, *15*, 313–319.
- (51) Dhami, S.; De Mello, A. J.; Rumbles, G.; Bishop, S. M.; Phillips, D.; Beeby, A. Phthalocyanine Fluorescence at High Concentration: Dimers or Reabsorption Effect? *Photochem. Photobiol.* **1995**, *61*, 341–346.
- (52) McRae, E. G.; Kasha, M. Enhancement of Phosphorescence Ability upon Aggregation of Dye Molecules. *J. Chem. Phys.* **1958**, *28*, 721–722.
- (53) Varghese, S.; Das, S. Role of Molecular Packing in Determining Solid-State Optical Properties of π -Conjugated Materials. *J. Phys. Chem. Lett.* **2011**, *2*, 863–873.

(54) Kono, S.; Fujimura, T.; Otani, Y.; Shimada, T.; Inoue, H.; Takagi, S. Microstructures of the Porphyrin/Viologen Monolayer on the Clay Surface: Segregation or Integration? *J. Phys. Chem. C* **2014**, *118*, 20504–20510.

(55) Stöter, M.; Biersack, B.; Reimer, N.; Herling, M.; Stock, N.; Schobert, R.; Brey, J. Ordered Heterostructures of Two Strictly Alternating Types of Nanoreactors. *Chem. Mater.* **2014**, *26*, 5412–5419.

(56) Suzuki, Y.; Himeno, D.; Tominaga, M.; Tani, S.; Nozaki, K.; Kawamata, J. Narrowing of X-ray Diffraction Peak of Clay-Organic Hybrid Films by Swelling and Drying Procedure. *Clay Sci.* **2015**, *19*, 79–83.

For Table of Contents Only

